Journal of Power Sources 249 (2014) 373–384

Contents lists available at ScienceDirect

Journal of Power Sources

journal homepage: www.elsevier.com/locate/jpowsour

In situ electrochemical studies of lithium-ion battery cathodes using atomic force microscopy

Sanjay Ramdon, Bharat Bhushan*, Shrikant C. Nagpure

Nanoprobe Laboratory for Bio- & Nanotechnology and Biomimetics, The Ohio State University, 201 W. 19th Avenue, Columbus, OH 43210, USA

HIGHLIGHTS

- Presented is review of in-situ electrochemical techniques for studying Li-ion battery.
- In-situ AFM allows accurate measurement of morphological changes during cycling.
- Li-wire cell design was chosen for ease of assembly in the glove box.
- During discharge, morphology showed an increase in particle size due to lithiation.
- In-situ AFM electrochemistry is useful for Li-ion battery degradation characterization.

GRAPHICAL ABSTRACT

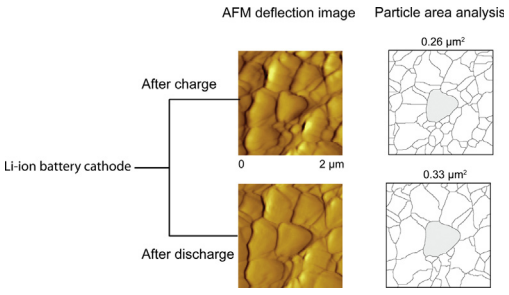

ARTICLE INFO

Article history:
Received 21 August 2013
Received in revised form
14 October 2013
Accepted 17 October 2013
Available online 1 November 2013

Keywords:
In situ electrochemical cell
Li-ion battery
$LiFePO_4$
Aging of cathode
Atomic force microscopy

ABSTRACT

Lithium-ion (Li-ion) batteries have been implemented for numerous applications, including plug-in hybrid electric vehicles (PHEV) and pure electric vehicles (EV). In an effort to prolong battery life, it is important to understand the mechanisms that cause reduced battery capacity with aging. Past studies have shown that morphological changes occur in aged cathodes. In situ electrochemical studies using atomic force microscopy allow for the direct observation of the morphology of the Li-ion battery cathode, at a nanometer scale resolution, during the cycling of an electrochemical cell. A simple electrochemical cell designed for in situ characterization is introduced. Charge/discharge curves and morphology data obtained during charging and discharging of cells are presented, and relevant mechanisms are discussed.

1. Introduction

Li-ion batteries have long been studied and developed as a power source for portable devices [1]. Since the early 2000s, Li-ion batteries have emerged as an energy storage medium for electric vehicles (EV), hybrid-EV (HEV) and plug in-EV (PHEV) in order to reduce the dependence on non-renewable energy sources. EVs are environmentally friendly because of their lower carbon emissions, and they are more economical to operate than conventional automobiles. Li-ion batteries are used in the automotive industry because of their extended life cycle, and because of their high energy density per unit weight (specific energy) [2,3].

Padhi et al. [4] first introduced lithium iron phosphate ($LiFePO_4$) as a Li-ion battery chemistry for cathode material. The $LiFePO_4$

* Corresponding author.
E-mail address: Bhushan.2@osu.edu (B. Bhushan).

0378-7753/$ – see front matter © 2013 Elsevier B.V. All rights reserved.
http://dx.doi.org/10.1016/j.jpowsour.2013.10.099

cathode has been of interest to researchers because of its coulometric capacity[1] per unit weight ($\approx$170 mAh g^{-1}), high thermal stability, specific energy ($\approx$0.60 Wh g^{-1}), and low toxicity [5–7]. $LiFePO_4$ is a viable option for meeting the requirements set by the United States Advance Battery Consortium (USABC) for the EV [8–10]. Over time, electrochemical properties of Li-ion batteries degrade, which leads to a reduction in storage capacity. Therefore, understanding the underlying mechanisms of the aging phenomenon in Li-ion batteries is of paramount importance in order to extend the life of Li-ion batteries [3,11].

Numerous ex-situ studies have been conducted to study the aging phenomenon in Li-ion batteries. These studies include atomic force microscopy (AFM), scanning electron microscopy (SEM), transmission electron microscopy (TEM), Raman spectroscopy, and other X-ray and neutron techniques [3,11]. These ex-situ studies were conducted by comparing the aged and unaged materials of cathodes and anodes in order to reveal morphological, electrical, and structural changes that occur during cycling. More specifically, studies on the $LiFePO_4$ battery cathode showed that $LiFePO_4$ nanoparticles agglomerate with age. During agglomeration the carbon coating on the particle needed for conductivity might degrade. Agglomeration is believed to result in an increase in surface resistance and a decrease in surface conductivity, which consequently reduces battery capacity [3,12,13]. Nanomechanical characterization experiments have been conducted to observe the effect of increased internal stress during aging [14]. Increases in creep and hardness were found to be associated with the degradation of the polyvinylidene fluoride (PVDF) binder and the formation of a dislocation due to the high internal stress and strain created during lithiation and delithiation. Although ex-situ studies resulted in some understanding of the aging phenomenon, a real time investigation of the battery electrodes during cell operation is only possible through in situ techniques.

In order to conduct in situ electrochemical measurements, custom built electrochemical cells that can operate inside an instrument must be utilized. Each experimental technique has its own set of difficulties associated with its operating conditions. For example, SEM and TEM require the sample to be in a vacuum, while AFM requires an open cell design that allows access to the electrode being investigated. AFM allows for the direct observation of the morphologies of Li-ion based electrodes at high resolution and on a nanometer scale [15–18].

In this work, a review of various in situ electrochemical cells used during Li-ion battery investigations is presented. Reasons for selecting AFM techniques are given. Different electrochemical cell designs used for in situ AFM experiments are described. Then a two-electrode electrochemical cell design is proposed, and the results of in situ AFM electrochemical studies on a $LiFePO_4$ battery cathode are presented.

2. Review of in situ electrochemical cells

Various in situ techniques have been applied to the study of Li-ion batteries, including optical, electron, AFM, neutron and X-ray techniques. Table 1 presents a summary of design requirements and comments on different electrochemical cells for each experimental technique. Schematics of cell designs are shown in Fig. 1(a)–(c). The following is a more detailed discussion of each technique and the in situ electrochemical cells utilized.

[1] The total Amp-hours available when the battery is discharged at a certain discharge current from 100% state-of-charge to the cut-off voltage. Capacity is calculated by multiplying the discharge current by the discharge time.

2.1. Optical

Optical methods include Raman microscopy and optical microscopy, which require a top cover that allows light to pass through, as shown in Fig. 1(a).

The Raman microscope technique is desirable for studying the structural and chemical composition of a sample. A Raman microscope is extremely useful for studying carbonaceous material, and it is useful for studying lithium intercalation through the carbon coating of cathodes [19]. Li^+ extraction and insertion has been observed on $LiNi_{0.8}$ $Co_{0.15}Al_{0.05}O_2$ cathodes [20]. The electrochemical cell used in this experiment was designed with a glass top cover to allow monochrome light to pass through. Panitz et al. [19] had a similar electrochemical cell design. They reported that when the thickness of the electrolyte layer was reduced from 0.5 mm to 0.2 mm, it resulted in an improved optical efficiency.

Though the optical in situ technique can only be utilized to probe morphological changes on the surface of the cathode, it does provide resolution on a micron scale [21]. An electrochemical cell utilized for the in situ optical microscopy technique is given in Fig. 1(a). Harris et al. [22] used the color change of graphite as an indicator of the extent of lithiation in order to obtain spatial profiles of Li intercalation. Quartz upper glass was used, however it was stated that lithium degrades the quartz material and a sapphire glass would yield better results.

2.2. Electron

The electron microscope can observe morphological changes on the nanometer scale. It requires an electrochemical cell with a transparent window to an electron beam. The experiments are conducted in a high vacuum and require electrolytes that are compatible, such as ionic liquids and solid electrolytes.

In situ TEM has been limited by the requirement of having ultrathin samples ($\sim$100 nm thickness) and a focused ion beam (FIB). TEM provides morphological, structural and compositional information using the techniques of imaging, diffraction and spectroscopy respectively [23]. Brazier et al. [24] were the first to conduct an ex-situ TEM observation of a solid state Li-ion battery. The first significant in situ electrochemical cell design was created by Liu and Huang [25] (also see Liu et al. [26]), which used ionic liquid electrolytes (ILEs). These electrolytes were shown to perform better in a high vacuum because of their ultra-low vapor pressure. Unocic et al. [27] created an in situ electrochemical cell that used a MEMS-based biasing microchip platform to seal the highly volatile electrolyte between two transparent electron SiN_x membranes. In order to improve spatial resolution, an energy-filtered transmission electron microscope (EFTEM) (to minimize chromatic aberrations) was used, followed by an electron energy loss spectroscope (EELS) to determine chemical changes.

In situ SEM studies were first performed by Orsini et al. [28]. Their electrochemical cell design did not allow for the cycling of the cell inside the SEM, thus the cycling was done outside of the SEM. After cycling, the cell was cooled down to -20 °C to pause the electrolyte degradation process, and then it was transferred to the SEM in an air-tight container. Raimann et al. [29] designed an electrochemical cell to have the least amount of evaporation of the electrolyte as possible by moderating the size of the exposed working electrode (pinhole diameter), the amount of electrolyte used, and the vacuum level inside of the SEM. However, this method reduced the resolution due to the scattering of electrons in the gas atmosphere that was created as the electrolyte evaporated. The problem faced when using conventional liquid electrolytes was eliminated [21] by using ionic liquids, which are very stable even in ultra-high vacuums because of their very low vapor pressure.

Table 1
In situ electrochemical cell for studying Li-ion batteries.

In-situ cell	Design requirement	Comments
Optical	Top cover transparent to visible light	
Raman microscope [20]		Structure and chemical composition at ~2 μm spatial resolution
Optical microscope [22]		Only shows morphological changes on microscale, low resolution
Electron	Window transparent to incoming electron beam. High vacuum required which limits electrolyte selection	Morphological changes on nanoscale can be measured
TEM [24]		Uses solid State Li-ion battery
Ref. [26]		Uses ionic liquid as electrolyte which has ultra-low vapor pressure
Ref. [27]		Cross section observation can be made. Sample used must be thin down to 100 nm thickness (FIB required)
SEM [28]		Battery cannot be cycled in SEM
Ref. [29]		Uses a lower vacuum (<10 Torr) than normal SEM which allowed use of electrolyte
Ref. [21]		Uses an ionic fluid which has low vapor pressure. Assemble of cell aided with nanomanipulator.
AFM	Clear path for access with probe	Can be used in ambient, however inert atmosphere required.
Ref. [15]		Continuous electrolyte flow. Reference and counter electrode outside of cell
Ref. [16,30]		Uses non flowing electrolyte
Ref. [18]		Continuous electrolyte flow with reference and counter electrode inside cell
Neutron	Window transparent to energy particle	Can quantify Li distribution and transport in battery during operation
Neutron depth profiling (NDP) [31]		Can measure Li concentration within the electrodes of the cell. To reduce resistance, the cell is heated before initial experiment.
Neutron reflectivity (NR) [33]		Measures neutron reflectivity intensity as a function of momentum transfer.
Small angle neutron scattering (SANS) [33]		Notable for measuring the structure variation in a sample through neutron scattering intensity
Neutron imaging (NI) [33]		
Neutron diffraction [34]		Wound cathode, electrolyte and anode stack
X-ray	Window transparent to X-ray	Can monitor detail structural changes
X-ray absorption spectroscopic (XAS) [35,36]	Kapton X-ray window	Completely sealed cell allows prolong monitoring. Provides detailed information on electronic structure and ordering.
Transmission X-ray microscope [37]		Can study structure and phase composition

2.3. AFM

The AFM microscope is a versatile tool for studying Li-ion batteries because high resolution images of the cathode surface can be obtained. Experiments can be completed under ambient conditions, but an inert atmosphere for electrochemistry is required. Electrochemical cell designs used during in situ AFM electrochemical studies on Li-ion batteries have very specific requirements to ensure good performance. Open access from the top of the cell is required to allow the AFM cantilever to enter into the cell and onto the working electrode. The materials used must not be reactive with the components of the cell. For example, because the electrolyte is very reactive, cell component materials that are chemically resistant are required such as Teflon®, which is often used in cell fabrication. The cell needs to be designed to accommodate the electrodes. The cell's counter and reference electrodes must be placed at precise locations that have stable electrical connections to the potentiostat.

Cells containing three-electrodes and two-electrodes with a continuous flow and a static electrolyte have been used. Vidu et al. [15] proposed a three electrode continuous flow electrochemical cell with the counter and reference electrodes located in an external reservoir, and with the working electrode located in the cell, as shown in Fig. 1(b). This entire setup is in an argon environment. Park et al. [18] used a different continuous flow cell than Vidu et al. [15]. In their design the lithium metal counter electrode was inside the electrochemical cell and the cell contained two electrodes [18]. Campana et al. [16], and Doi et al. [17] (also see Inaba et al. [30]) used a non-flow electrolyte and three-electrode systems in which the counter and reference electrodes were placed in an enclosed cell. The area of the working electrode was confined by an O-ring, which prevented the electrolyte from leaking.

2.4. Neutron techniques

There are several neutron techniques shown in Fig 1(c), including neutron depth profiling (NDP), neutron reflectivity (NR), small angle neutron scattering (SANS), neutron imaging (NI), and neutron diffraction. These techniques require an electrochemical cell that is transparent to energy particles, and that can be used to quantify the Li distribution and transportation within the battery.

NDP is a powerful technique for measuring Li-ion concentration deep in the sample. Oudenhoven et al. [31] developed an in situ electrochemical cell for NDP applications that is shown in Fig. 1(c). This cell design requires heating the electrolyte to 250 °C, then maintaining this temperature for 10 min in order to reduce the resistance to the electrolyte at the interface by a factor of 2. This cell design is similar to that of Neudecker et al. [32].

Neutron reflectivity (NR) is most notable for measuring volume expansion and retraction on electrodes, as stated by Wang et al. [33]. The intensity of the NR is measured as a function of the momentum transfer. The NR electrochemical cell shown in Fig. 1(c) uses Li-metal in the counter and reference electrodes. Its electrolyte is enclosed by a Viton® O-ring that also confines the working electrode. Gold foil is used to make connections to the electrodes.

Small angle neutron scattering (SANS), shown in Fig. 1(c), measures the neutron scattering intensity as a function of the momentum transfer velocity [33]. This instrument is notable for measuring the structural variations in a sample. Li-metal is used in the reference and counter electrodes. The working electrode is comprised of graphite. The cell is also designed with quartz windows on the top and bottom to allow the neutron beam to pass through the cell.

Neutron Imaging (NI) shown in Fig. 1(c), measures the spatial changes in the transmission of Li relative to a reference [33]. NI may help to construct more accurate circuit models when

designing rechargeable batteries in the future. Neutron diffraction measurements are performed on a specially designed electrochemical cell that contains a wound cathode, an electrolyte, and an anode sealed in a quartz or aluminum tube [34]. This was chosen to allow for a constant path length for neutron absorption.

2.5. X-ray techniques

X-ray absorption spectroscopy (XAS), shown in Fig. 1(c), is used for the monitoring of the structural composition of an electrode. This is the preferred technique for obtaining detailed information on electronic structure and order [35,36]. The cell is completely sealed, thus allowing monitoring for an extended period of time. A Kapton® foil is used as the window in this cell design because the window must be transparent to X-rays. A transmission X-ray microscope is used for studying structural and phase compositions. The in situ cell is made in a manner similar to a coin cell, however there is a hole through the top and bottom cover of the in situ cell that is sealed with Kapton® [37].

2.6. Selection of the technique used in the present study

AFM was selected for this study because it does not require samples to receive any special treatments that could cause changes or damage, such as the conductive coating required in electron microscopy. AFM does not require an ultra-high vacuum environment to operate. Conventional electrolytes, such as a hexafluorophosphate ($LiPF_6$) salt in an alkaline carbonate solvent, can be used. AFM provides high resolution morphological information for samples, and it can perform well in a liquid environment.

3. Experimental details

The proposed experimental cell was placed inside a glove box with an argon atmosphere. It was cycled using a potentiostat.

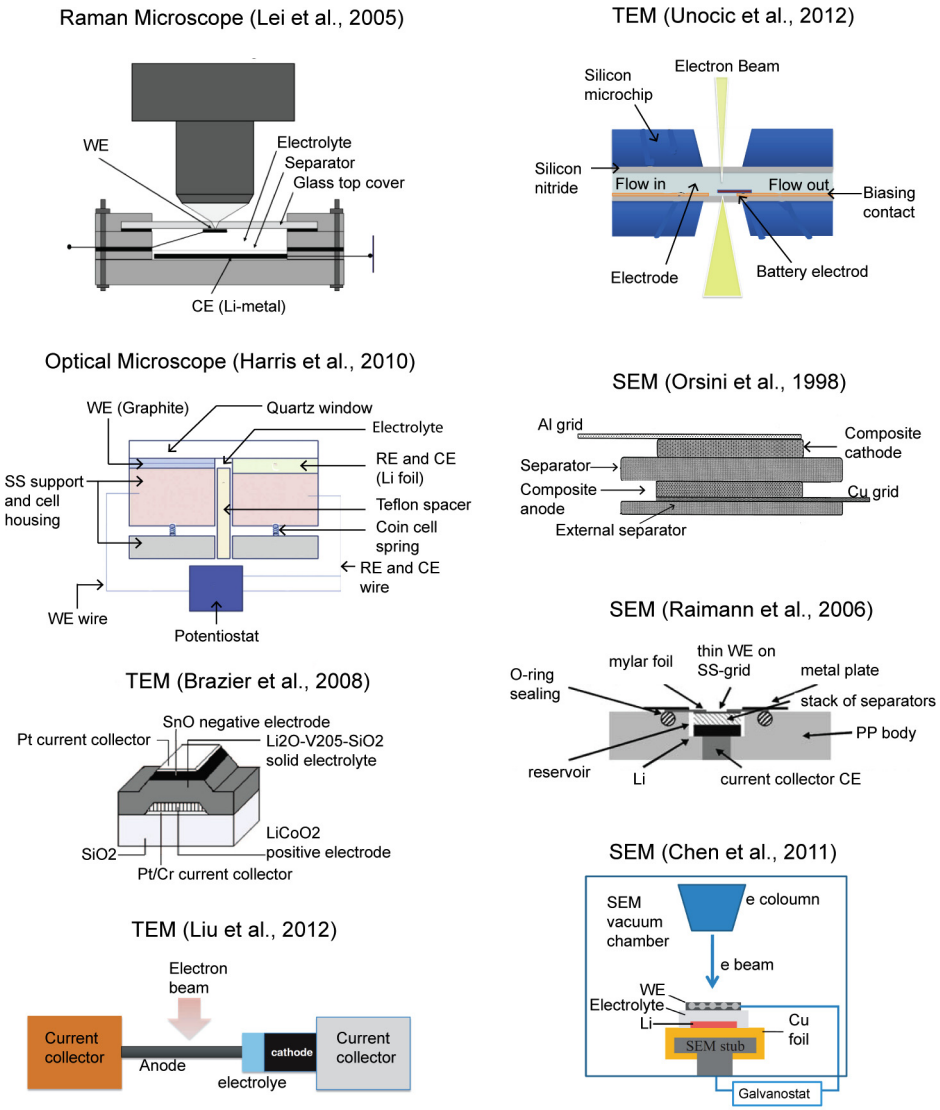

Fig. 1. Schematics of In situ electrochemical cells for (a) Raman [20], optical [22] and transmission electron microscope (TEM) [24,26,27] and scanning electron microscope (SEM) [21,28,29], (b) AFM [15,16,18,30], and (c) for neutron [31,33,34] and X-ray [36,37] experimental techniques. WE, CE and RE represent working electrode, counter electrode and reference electrode respectively.

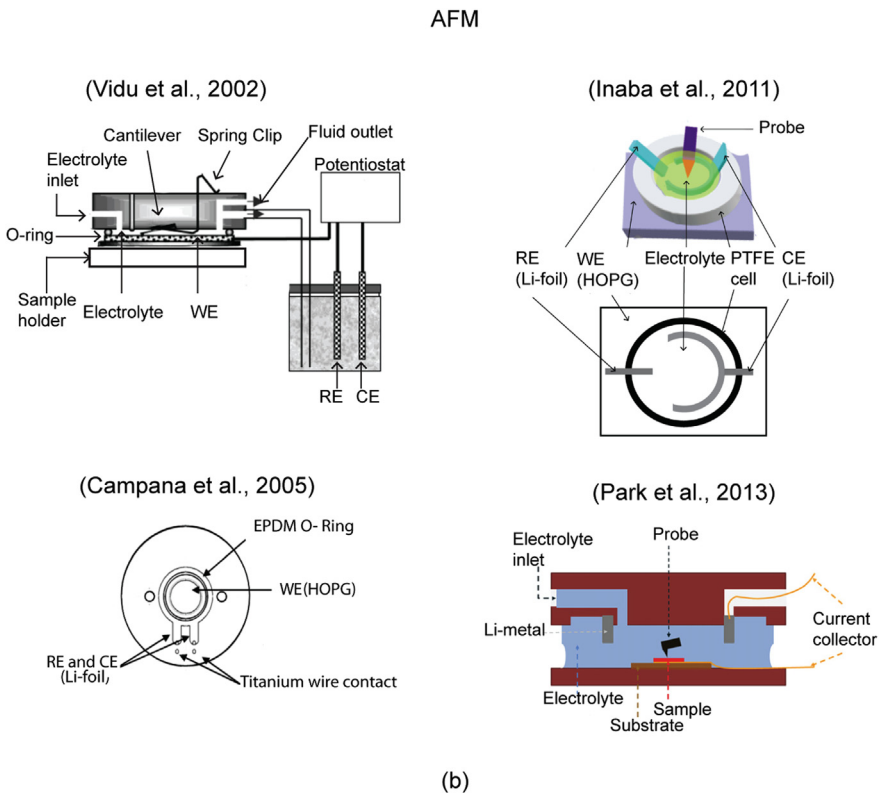

Fig. 1. (*continued*).

During cycling, AFM was used to investigate any morphology changes.

3.1. AFM, glove box and potentiostat

Fig. 2(a) shows the schematic of the Agilent 5500 AFM head (Agilent Technologies, Chandler, AZ). The main components of the AFM head are a laser diode, a piezo scanner, a cantilever, and a quad diode laser detector [38]. The sample is mounted under the AFM head below the cantilever. The cantilever tip assembly is mounted to the lower end of the piezo scanner. The piezo scanner consists of three separate electrodes that precisely scan the sample in the x–y plane in a raster pattern and that move the sample in the vertical (z) direction. A sharp tip at the free end of the cantilever is brought into contact with the sample. Features on the sample surface cause the cantilever to deflect in vertical and lateral directions as the piezo scans the tip over the surface. A laser beam from a laser diode is directed onto the back of the cantilever near its free end, tilted downward at about 9° with respect to the horizontal plane. The cantilever is coated in gold on the detector side to enhance laser reflection. The reflected beam from the vertex of the cantilever is directed onto a quad diode laser detector.

Topographic features of the sample cause the tip to deflect in a vertical direction as the sample is scanned under the tip. This tip deflection will change the direction of the reflected laser beam, thereby changing the intensity difference between the top and bottom sets of the diode laser detectors (AFM signal). A feedback circuit is used to modulate the voltage applied to the piezo scanner and to adjust the height of the piezo. This feedback system ensures that vertical deflection from the cantilever (given by the intensity difference between the top and bottom detector) remains constant during scanning. The feedback signal is used to create the AFM height image, while the raw deflection signal creates the deflection image. The deflection image provides a good lateral resolution for particles or other features, and the height image gives accurate height information.

A balanced pendulum method is used as part of the design of this AFM head. This means the laser diode, piezo and cantilever are all fixed together and move as a balanced pendulum. This allows the laser tracking spot to remain fixed onto the cantilever. Other AFM systems use a lens system to track the laser spot on the cantilever while the cantilever moves independently. This causes artifacts at the end of large scan size images. The balanced pendulum design also lowers the moment of the inertia on the piezo, thus reducing noise in the system.

The glove box used, shown in Fig 2(b), is designed with two compartments: one compartment for storage is on the left and the other compartment for in situ AFM electrochemical experiments is on the right. They both are independently sealed with a transfer chamber in between, which allows for the transfer of items to and from storage while performing experiments. The glove box has ports used to connect the electrical connections to the potentiostat for cycling. The AFM is mounted through a circular hole at the top, which provides a good seal for the argon environment. In situ experiments were conducted in an ultra-high purity argon (99.998%) filled glove box maintained at a slightly positive pressure (~10 Pa), and equipped with drierite moisture absorbent material (W.A. Hammond Drierite. CO. LTD, Xenia, OH). The potentiostat used is the Gamry Reference 600 (Gamry Instruments, Warminster, PA).

3.2. In situ cell design

As presented earlier, three-electrode and two-electrode cell designs have been used in previous work. In these studies the three-electrode cell design has separate counter and reference

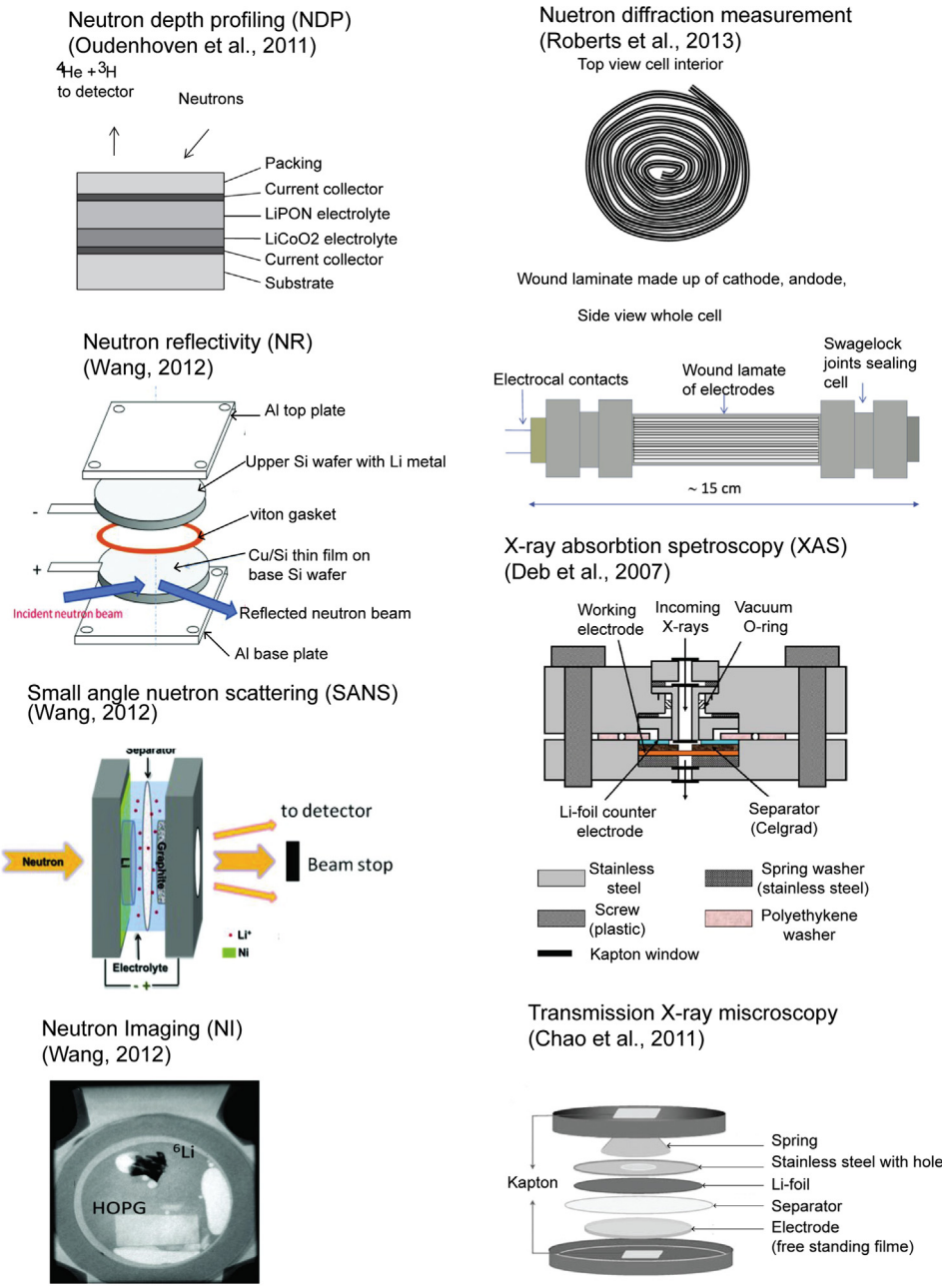

(c)

Fig. 1. (*continued*).

electrodes and the two-electrode cell design has the same electrode for both counter and reference electrodes.

The schematic of a three-electrode cell is shown in Fig. 3(a) top. The working electrode (WE), reference electrode (RE) and counter electrode (CE) as well as the electrolyte and the potentiostat electrical connection are shown. The WE is typically where the sample is tested, it is where the potential is controlled, and where the current is measured. The RE is used in measuring the WE electrode potential and it is normally kept at a constant electrochemical potential. The CE completes the circuit. The current flowing through the solution enters through the WE and leaves through the CE.

For in situ AFM electrochemistry, an open cell design is needed to perform AFM imaging. A three-electrode commercial electrochemical cell design (Agilent N9410A-OC-LIQUID) is shown in Fig. 3(a) bottom. The working electrode has a confined area for the electrolyte using an O-ring and a spring loaded pin and clip mechanism. The cell is designed to accommodate a rigid wire of about 0.5 mm in diameter for the counter and reference electrodes. In the case of Li-ion batteries, Li-metal is needed for the counter and reference electrodes. Li-metal is soft, and since it is not rigid it will not remain in place. Furthermore, this cell design has a shallow reservoir, so the electrolyte will evaporate in a shorter time than the experiment duration of several hours.

To simplify the assembling process of the cell in the glove box, a two-electrode setup is used as shown in Fig. 3(b) top. The schematic of the proposed in situ AFM electrochemical cell is

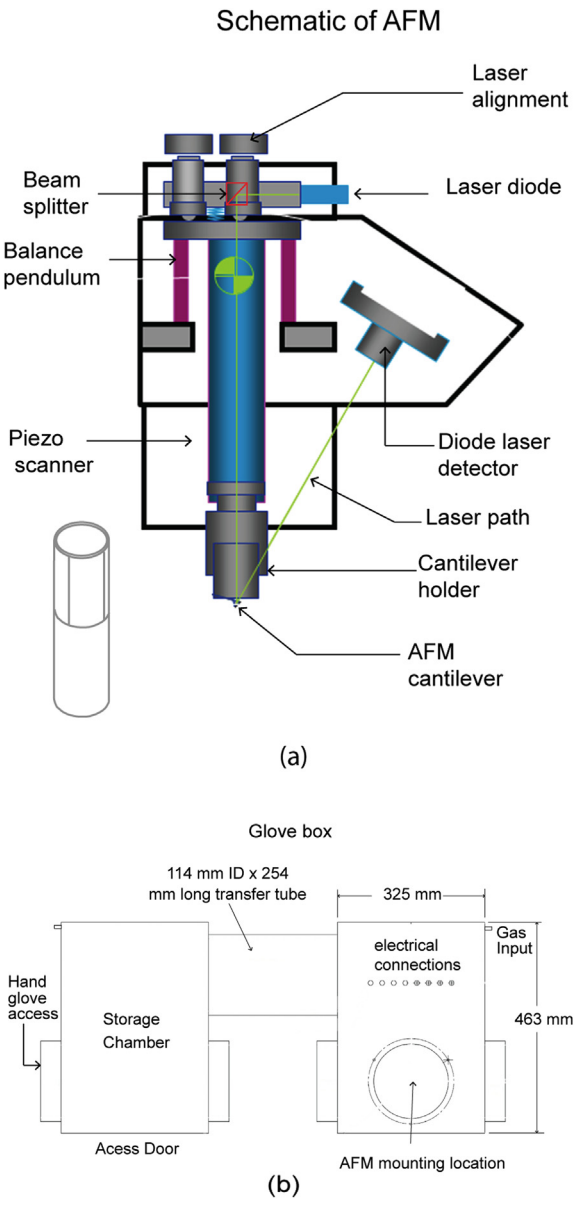

Fig. 2. Schematics of (a) AFM and (b) glove box designed for storage as well as electrochemical experiments.

shown in Fig. 3(b) middle and bottom. The Li-wire cell design shown in Fig. 3(b) middle is a modification of the design discussed earlier. It uses a deeper cup to hold larger quantities of electrolyte, and it has an opening which allows for the easy insertion of the flexible Li-wire without obstructing the AFM head. It uses counter and reference electrodes consisting of Li-wire, and it uses a Li-ion cathode as the working electrode submerged in an electrolyte. A Teflon® cup with a hole through the side (~3 mm) for the Li-wire is used. A copper metal rod with a plate for mounting the sample is placed through the base of the cup, and it is sealed by a Viton® O-ring. The inner diameter of the cell opening is 30 mm and 8 mm in depth.

The other design is a coin cell design as shown in Fig. 3(b) bottom. It uses a Li-foil with an opening in the middle as the reference and counter electrode. The working electrode is separated from the Li-foil with a separator. The cell components are assembled in the lower cell casing with a spring and spacer below the working electrode used for making an electrical connection from the working electrode to the lower casing of the cell. A few drops of electrolyte are dropped into the cell before another spacer with an opening is placed on top of the Li-foil. Then the top cover with an opening is placed as the cover for the cell. This assembly is then crimpled shut in a crimping machine.

The wire AFM electrochemical cell in Fig. 3(b) middle was chosen to conduct the experiments in this paper. It does not have numerous parts or require the punching of separators and lithium, nor does it necessitate a crimping machine. Li-wire was used for the counter and reference electrodes. The Li-wire can be handled more easily in the glove box and it does not need additional preparation before the cell is assembled.

A description of the steps taken to assemble the cell follows. First the Teflon® cup with a copper metal rod through its base and the Teflon® O-ring are cleaned. These components are placed in a beaker that is then filled with isopropyl alcohol and sonicated for 15 min. Next the components are dried in an oven at 75 °C for approximately 12 h. The components are then transferred to the glove box, which is purged three times with argon. A working electrode of about 15 mm in diameter that was cut from a commercial battery cathode is affixed to the copper plate at the top of the copper rod. The working electrode is attached using an oversized Teflon® O-ring in order to keep it in position. The use of the copper did not change the electrochemical performance of the cell as compared to using aluminum as a current collector. An electrolyte of 1 M $LiPF_6$ salt in 1:1 ethylene carbonate/dimethyl carbonate (Novolyte technologies, Zachary, LA) was used to fill the cell to $^3/_4$ capacity (about 4 cm^3), allowing room for the AFM probe and preventing spillage.

3.3. Extraction of samples from a commercial cell

Cylindrical Li-ion cells used in the experiments have cathode material on an aluminum current collector made of $LiFePO_4$ nanoparticles. These nanoparticles are coated with carbon for increased conduction. They are mixed in a slurry of polyvinylidene fluoride (PVDF), which acts as the binder. The graphite on a copper current collector is used as the anode, and lithium hexafluorophosphate ($LiPF_6$) salt in an alkaline carbonate solvent is used as the electrolyte. The anode and cathode are separated by a separator, and then rolled in a tube to create the cell. The cell has an operating voltage of 3.3 V and a nominal discharge capacity of 2.3 Ah.

The cell was charged and discharged completely at 1C (1C = 2.3 Ah) to verify its capacity. Next, the cell was disassembled in air, and long strips of cathode were extracted. One side of the extracted cathode was cleaned using 1-methyl 2-pyrrolindinone (Sigma Aldrich, St. Louis, MO) to remove $LiFePO_4$ and to expose the aluminum current collector.

3.4. A commercial cell for comparison

The commercial cell ANR26650 (A123 Systems, Inc, Waltham, MA) was used as a reference for data obtained from the experimental wire cell. It has a charge/discharge capacity of 2.5 Ah, and an operating voltage of 3.3 V. It was completely charged and discharged using the potentiostat at a charge/discharge rate of C/6. The current for a C/6 rate was obtained by dividing the charge/discharge capacity of 2.5 Ah by 6 to obtain ±0.417 A. This C/6 rate was chosen to be similar to the rate used during the in situ AFM experiments to be described later, in order to serve as a suitable reference.

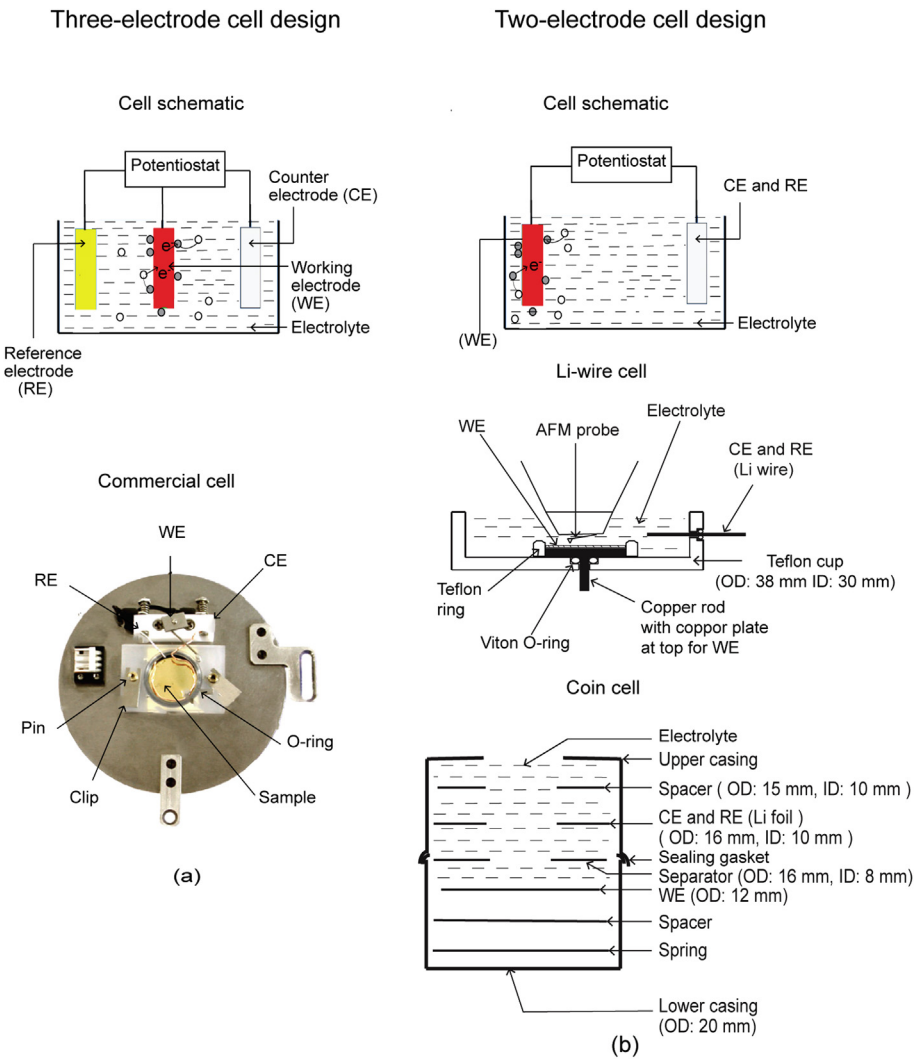

Fig. 3. AFM electrochemical cell designs proposed for in situ electrochemical experiments, (a) three-electrode with cell schematic (top) and commercial cell (bottom), and (b) two-electrode cell design with cell schematic (top), Li-wire cell (middle) and coin cell (bottom).

3.5. *In situ AFM experiment*

The cell was cycled three times using a potentiostat, known as a formation cycle, before the start of the experiment. This was done to allow the cell to stabilize its charge/discharge capacity, as well as to develop a solid electrolyte interphase (SEI) layer. After the formation cycle, the in situ AFM experiment was conducted. Before the cell was charged AFM height and deflection images were taken, then after charging the cell by applying a positive current these images were taken again. The cell was then discharged by applying a negative current, and post discharge AFM images were taken. The AFM images were taken in contact mode using a silicon probe with a 70 nm thick gold reflective coating (Budget Sensor ContGD), a force constant of 0.2 N m^{-1}, and a resonant frequency of 13 kHz. An AFM scan speed of 2 Hz was used to obtain an image with a scan size of 2 μm × 2 μm. It took about 15 min to complete an image. AFM images were then processed using Agilent Pico Image Expert software, and particles were analyzed using the particle size analysis feature.

A suitable C-rate was selected for the experiments. The C-rate is a measurement of the rate at which a cell is charged and discharged relative to its capacity. A charge rate of 1C means that it would take 1 h to charge the cell and 1 h to discharge the cell if it is discharged at a current of 2.3 A. Initial experiments at 1 C and C/6 rates showed that more changes in morphology were observed at C/6 rate (6 h test duration) as a result of cycling. The underlying reason for this phenomenon is, due to its design there is an opening in the in-situ cell to accommodate the AFM probe; therefore de/intercalation of Li ions takes more time since the diffusion path in the electrolyte is longer and the Li counter electrode surface area is smaller than the cathode (i.e., working electrode) surface area. As a result, an in-situ cell does not work properly at higher C rates (i.e., >C/6). On the other hand, slower C rates result in more electrolyte evaporation since charging/discharging takes more time. Therefore, C/6 rate was selected since it is the optimal value to limit the excessive electrolyte evaporation and it gives Li ions enough time to diffuse in and out of the cathode. Park et al. [18] reported a C-rate of C/10.

The theoretical capacity of the experimental wire cell is needed in order to set the C-rate for the charge/discharge current used to cycle the cell. In order to calculate the theoretical capacity of the experimental wire cell, the capacity per unit area of the original complete cell was calculated and multiplied by the total area of the working electrode of the experimental cell. The capacity per unit area of the original complete cell for 1C-rate is obtained by dividing its capacity specified by the manufacturer (2.3 Ah) by the total area of the cathode material on both its sides (152.4 cm × 6.35 cm × 2 = 1935 cm^2), and is

equal to 1.189 mAh cm^{-2}. The theoretical capacity of the experimental wire cell for 1C-rate can then be calculated by multiplying this capacity per unit area by the area of the working electrode in the experimental wire cell (1.65 cm^2), and is equal to 1.96 mAh. For the selected C/6 charge rate, the theoretical capacity value was obtained by dividing it by six to give ±327 μAh.

Pico Image Expert image analysis software (Agilent Technologies, Chandler, AZ) was used to analyze the particle diameter. The software employs a specific algorithm to determine the peaks and the associated valleys for a particle. Then a segmentation method is applied to select the particle boundary. The selection can then be more precisely tuned, depending on the particle of interest, by changing the height threshold setting and the area of particle selection setting.

4. Results and discussion

Experiments conducted on a commercial Li-ion battery that will serve as a reference for the in situ AFM wire experimental cell are presented. AFM images of the bare cathode and the cathode in an electrolyte are presented as a means of discussing the impact of the electrolyte on imaging. The cell was charged and discharged at a C/6 rate, which should take 6 h to charge and 6 h to discharge. In situ AFM images of the experimental wire cell during charging and discharging are also presented in order to study the morphological changes that occur.

4.1. Charge/discharge curves of the commercial cell and the experimental wire cell

The theoretical charge/discharge capacity of the commercial cell is 2.5 Ah, whereas the measured capacity of the battery was calculated to be 2.6 Ah. This was calculated by multiplying the applied current by the time taken to completely discharge the cell. This calculation was done to verify the manufacturer's rated capacity and to gauge the performance of the cell. The difference in capacities could be due to the lower and upper limits of the cell used by the manufacturer when determining the cell's charge/discharge capacity.

Charge and discharge curves were obtained on a commercial $LiFePO_4$ cell to provide a reference to that of the experimental wire cell. The charge and discharge curves are shown Fig. 4. The cell was

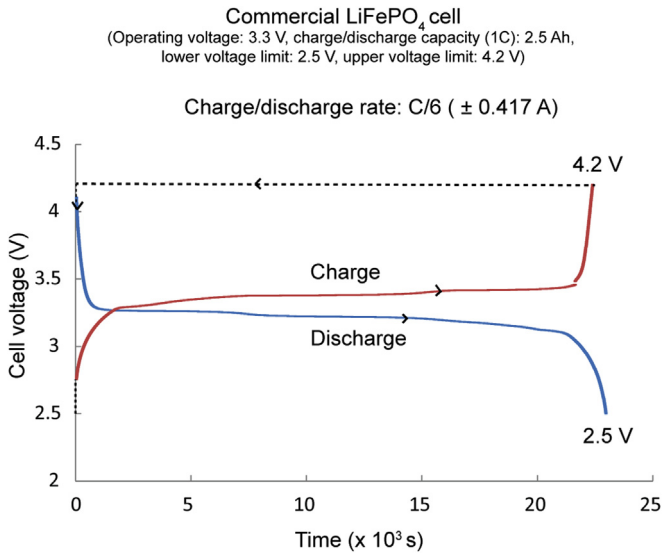

Fig. 4. Charge and discharge curve of a commercial $LiFePO_4$ cell.

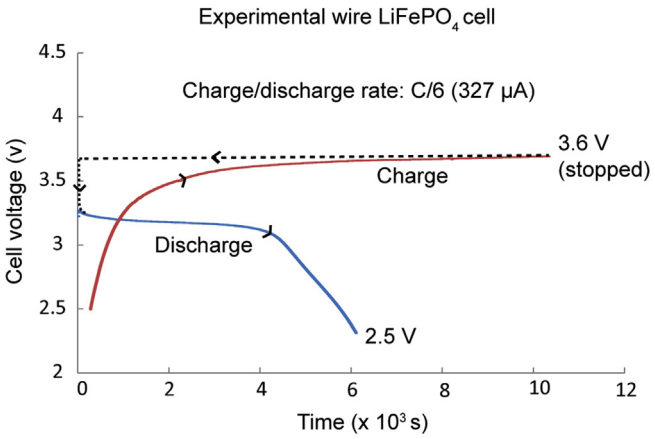

Fig. 5. Charge and discharge curve of an experimental wire $LiFePO_4$ cell.

charged from the lower limit of 2.5 V to the upper limit of 4.2 V. During charging the voltage of the cell rapidly increased from 2.5 V to 3.29 V, where it increased steadily over 5.5 h until the voltage reached 3.44 V, then it increased rapidly to the upper limit of 4.2 V. The discharge was then started immediately, with a beginning charge of 4.1 V. In Fig. 4 the gap between the ideal starting discharge voltage and the voltage found in this experiment is represented by the dotted line, which shows where the voltage curve should have started in an ideal case. The voltage rapidly dropped to 3.28 V, which is slightly below the operating voltage of the cell of 3.3 V. The cell then gradually discharged at a steady rate over 5.5 h until it reached 3.1 V, at this point it decreased rapidly until reaching the lower limit of 2.5 V.

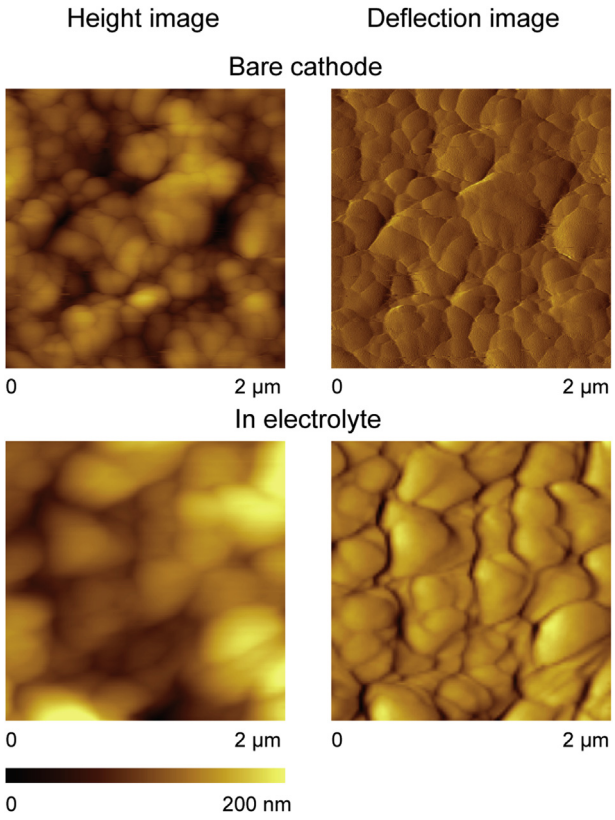

Fig. 6. AFM height and deflection image of bare and in electrolyte $LiFePO_4$ cathode.

The cycling of the Li-wire cell data are shown in Fig. 5. Based on the available lifetime limitation of the cell, it was stopped 2.7 h into charging. The discharge of the cell reached the lower limit of 2.5 V in 1.7 h. At the start of charging the cell the voltage increased gradually over 1 h, and then it gradually leveled to the limit of 3.6 V for the remaining time. The discharge was started immediately after charging was stopped. The starting discharge voltage was 3.27 V. In Fig. 5 the dotted line shows the drop in voltage from charging to discharging, and it shows where the discharge curve should have started in an ideal case. The cell's voltage reduced gradually to 3.1 V, and then reduced more rapidly to the set lower limit.

The commercial cell's charge and discharge curves were as expected from the theoretical calculations. The theoretical capacity was similar to the experimental capacity. The experimental wire cell showed a larger drop in voltage from the end of discharging to the start of charging, and discharging occurred much faster than the theoretically calculated discharge time. This result may be because the cell is open and the electrolyte volume in the cell is slowly reducing over time. Therefore, the concentration of the electrolyte is changing.

4.2. AFM images of the bare cathode and the cathode in the electrolyte

Representative AFM images of the bare cathode and the cathode in the electrolyte are shown in Fig. 6. The AFM image of the cathode in the electrolyte is slightly noisier than that of the bare cathode. The boundary of the particles shown in the deflection image of the bare cathode is better defined than the particle boundary in the deflection image of the cathode in the electrolyte.

4.3. In situ AFM images of cathode during charge and discharge

Fig. 7 shows height and deflection images, as well as the particle area analyses of the cathode, initially and after both charging and discharging. A visible change in the shape of the particles was observed in the images collected before and after charging. The particles became more rounded. After discharging the cell, the shapes of the particles became more similar to the shapes initially observed. The particles appear visually larger after discharging than after charging.

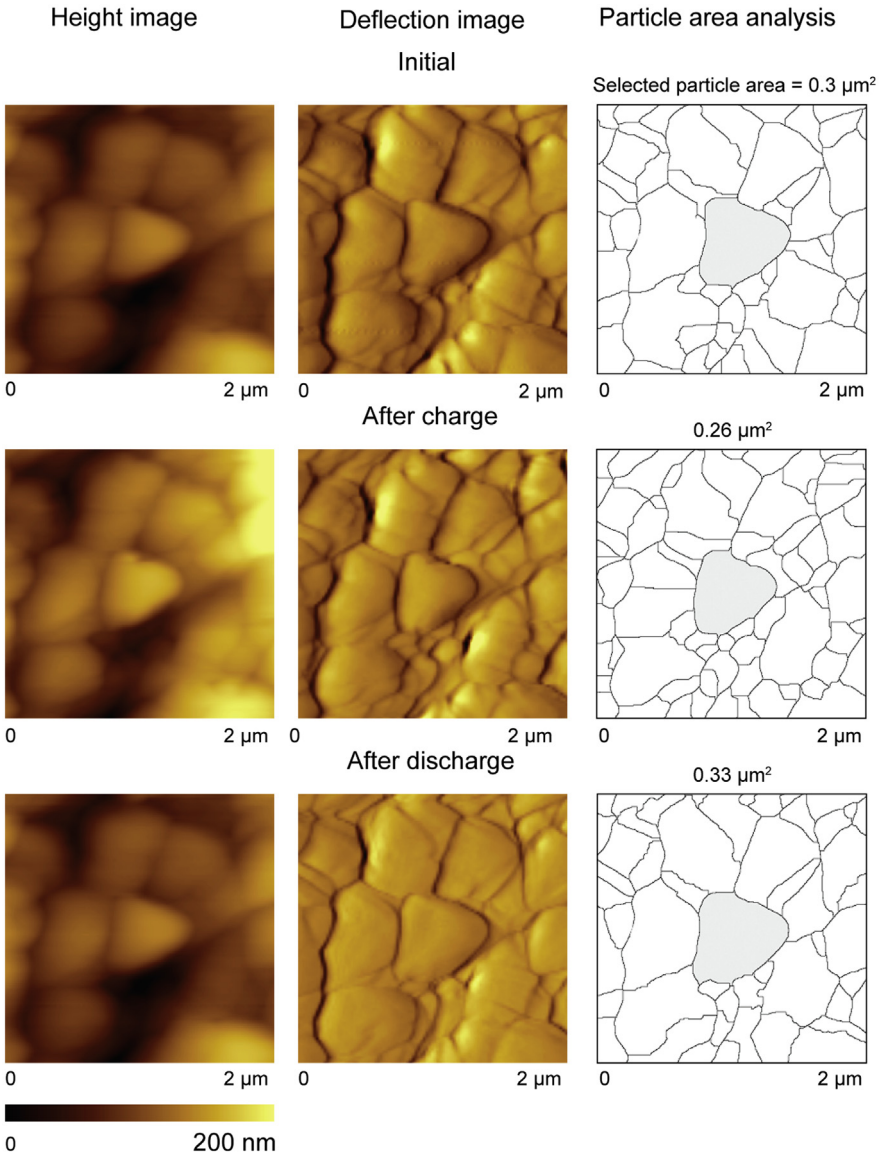

Fig. 7. AFM height and deflection image as well as particle area analysis of $LiFePO_4$ cathode showing change of particle size between charged and discharged states.

Particle analysis was then done to quantify the changes in the size of the particle, as shown in Fig. 7. The particle selected had a distinct shape and outline. The particle was also visually separate from the surrounding particles and had a distinct boundary. This selection process facilitates the proper selection of a particle by the image analysis software, and produces accurate results. The particle chosen was highlighted, and the area of the particle was determined from the software. The area of the initial particle chosen is 0.3 μm^2. After charging, the area of the particle was reduced to 0.26 μm^2. The cell was then discharged as shown in Fig. 5, and an image was taken. The particle size changed from 0.26 μm^2 to 0.33 μm^2 after discharging with a change on the order of 25%. This result shows that an increase in the size of the particle from fully charged to fully discharged exists. This increase is due to the phase change of the particle from the $FePO_4$ phase to the $LiFePO_4$ phase as described below.

To understand what is occurring within the cathode as the cell is charged and discharged it is important to examine the morphological changes shown in Fig. 7. Srinivasan and Newman [39] described this in the form of a shrinking core model. In a fully charged cell there exist single phase $FePO_4$ particles in the cathode. As the discharge is started, a reaction begins on the surface of the $FePO_4$ particle, and the Li^+ moves from the anode to intercalate into the cathode. The $FePO_4$ particle then changes to a $LiFePO_4$ particle. The Li^+ intercalates into the lattice of the $LiFePO_4$ particle, eventually creating phase segregation between the Li-rich region (outer shell) that has a high Li content and the Li-deficient region (inner core). As discharge continues, a greater amount of Li is inserted into the lattice, there it intercalates to the Li-deficient region. This eventually will change the entire particle into one Li-rich region. The particle will then be fully converted into $LiFePO_4$. The reverse occurs during charging. The total unit volume change between the $FePo_4$ phase and the $LiFePO_4$ phase is 6.8% [4].

5. Conclusions

A review of various in situ electrochemical cells for a Li-ion battery investigation is presented. An AFM technique was chosen for this study because it provides high resolution morphological information for samples, it performs well in a liquid environment, and it requires no special sample preparation. It also does not need an ultra-high vacuum environment to operate. Various electrochemical cell designs using an AFM are described. A wire experimental cell design was chosen because fewer parts were required, thus making assembly in the glove box easier. Lithium wire could also be handled easily without needing any extra preparation. In situ electrochemical AFM studies on the Li-ion battery allow for the accurate measurement of the morphological changes that occur on the cathodes during cycling of the cell at a nanometer scale resolution.

Charge/discharge curves were different for the commercial cell used as a reference than that of the experimental cell. The commercial cell operated as expected from theoretical calculations. The experimental wire cell showed a larger drop in voltage from the end of discharging to the start of charging, and it discharged much faster than the theoretically calculated discharge time. Morphology data, shown in Fig. 7, shows an increase in particle size from the $FePO_4$ phase to the $LiFePO_4$ phase during the discharge of the cell. This increase in particle size was due to lithiation, and occurred as expected. The particle size reduced from an initial size of 0.30 μm^2 to a size of 0.26 μm^2 when charged, and after discharging the monitored particle size increased from 0.26 μm^2 to 0.33 μm^2.

In situ AFM electrochemical experiments provide useful information about morphological changes during charging and discharging. These experiments can be used for further Li-ion battery characterization. The Li-wire cell design has a large electrolyte area exposed to ambient conditions, which leads to the evaporation of the electrolyte. Hence, a more suitable design may be needed.

Acknowledgment

This material is based upon work supported by the Department of Energy, Washington, DC, under Award Number DE-PI0000012. Authors would like to sincerely thank Dr. Song Xu for providing instrumentation support during the beginning of this work and Dr. D. Emre Demirocak for providing technical discussions during the completion of this work as well as critical review of the manuscript. The authors would also like to express sincere gratitude to the members of NLBB.

References

[1] M. Armand, J.M. Tarascon, Nature 451 (2008) 652–657.
[2] S.C. Nagpure, B. Bhushan, in: B. Bhushan, H. Fuchs (Eds.), Applied Scanning Probe Methods – Biomimetics and Industrial Applications, vol. 13, Springer, Heidelberg, Germany, 2009, pp. 203–233.
[3] S.C. Nagpure, Multi-scaled Characterization of Aged Li-ion Battery Materials for Improving Performance (Ph.D. Thesis), The Ohio State University, Department of Mechanical and Aerospace Engineering, Columbus, Ohio, 2011.
[4] A.K. Padhi, K.S. Najundaswamy, J.B. Goodenough, J. Electrochem. Soc. 144 (1997) 1188–1194.
[5] W. Borong, Y. Ren, L. Li, in: S. Soylu (Ed.), Electric Vehicles – the Benefits and Barriers, InTech, Europe, 2011, pp. 199–202.
[6] D. Choi, W. Wang, Z. Yangin, in: X. Yuan, L. Liu, J. Zhan (Eds.), Lithium-ion Batteries: Advanced Materials and Technologies, CRC Press, New York, 2012, pp. 1–16.
[7] K. Zaghib, A. Mauger, J.B. Godenough, C.M. Julien, in: Y. Abu-Lebdeh, I. Davidson (Eds.), Nanotechnology for Lithium-ion Batteries, Springer, Heidelberg, Germany, 2013, pp. 179–182.
[8] Anonymous, FreedomCAR 42 V Energy Storage System End-of-life Performance Goals, USABC, Southfield, MI, 2002. Available from: <http://www.uscar.org/guest/view_team.php?teams_id=12>.
[9] Anonymous, USABC Goals for Advanced Batteries for EVs, USABC, Southfield, MI, 2006a. Available from: <http://www.uscar.org/guest/view_team.php?teams_id=12>.
[10] Anonymous, USABC Requirements of End of Life Energy Storage Systems for PHEVs, USABC, Southfield, MI, 2006b. Available from: <http://www.uscar.org/guest/view_team.php?teams_id=12>.
[11] S.C. Nagpure, B. Bhushan, S. Babu, J. Electrochem. Soc. 160 (2013) A2111–A2154.
[12] S.C. Nagpure, B. Bhushan, S. Babu, G. Rizzoni, Script. Mater. 60 (2009) 933–936.
[13] S. Ramdon, B. Bhushan, J. Colloid Interface Sci. 380 (2012) 187–191.
[14] S. Ramdon, B. Bhushan, J. Power Sources 246 (2014) 219–224.
[15] R. Vidu, F.T. Quinlan, P. Stroeve, Ind. Eng. Chem. Res. 41 (2002) 6546–6554.
[16] F.P. Campana, R. Kotz, J. Vetter, P. Novak, H. Siegenthaler, Electrochem. Commun. 7 (2005) 107–112.
[17] T. Doi, M. Inaba, H. Tsuchiya, S.K. Jeong, Y. Iriyama, T. Abe, Z. Ogumi, J. Power Sources 180 (2008) 539–545.
[18] J. Park, S. Kalnaus, S. Han, Y.K. Lee, G.B. Less, N.J. Dudney, C. Daniel, A.M. Sastry, J. Power Sources 222 (2013) 417–425.
[19] J.C. Panitz, P. Novak, O. Haas, Appl. Spec. 55 (2001) 1131–1137.
[20] K.L. Lei, F. McLarnon, R. Kostecki, J. Phys. Chem. B 109 (2005) 952–957.
[21] D. Chen, S. Indris, M. Schulzc, B. Gamera, R. Mönіga, J. Power Sources 196 (2011) 6382–6387.
[22] S.J. Harris, A. Timmons, D.R. Baker, C. Monroe, Chem. Phys. Lett. 485 (2010) 265–274.
[23] Y.S. Meng, T. McGilvray, M.C. Yang, D. Cotovic, F. Wang, D. Xeng, Y. Zhu, J. Greatz, Electrochem. Soc. Interface Fall (2011) 49–52.
[24] A. Brazier, L. Dupont, L. Dantras-Laffont, N. Kuwata, J. Kawamura, J.M. Tarascon, Chem. Mater. 20 (2008) 2352–2359.
[25] X.H. Liu, J.Y. Huang, Energy Environ. Sci. 4 (2011) 3844–3860.
[26] X.H. Liu, Y. Liu, A. Kushuma, S. Zhang, T. Zhu, J. Li, Y. Huang, Adv. Energy Mater. 2 (2012) 722–741.
[27] R.R. Unocic, L. Baggetto, K.A. Unocic, G.M. Veith, N.J. Dudnet, K.L. More, Mocrosc. Microanal. 18 (2012) 1104–1105.
[28] F. Orsini, A. Du Pasquier, B. Beaudoin, J.M. Tarascon, M. Trentin, N. Langenhuizen, E. De Beer, P. Notten, J. Power Sources 76 (1998) 19–29.
[29] P.R. Raimann, N.S. Hochgatterer, C. Korepp, K.C. Möller, M. Winter, H. Schröttner, F. Hofer, J.O. Besenhard, Ionics 12 (2006) 253–255.
[30] M. Inaba, S.K. Jeong, Z. Ogumi, Electrochem. Soc. Interface Fall (2011) 55–59.
[31] J.F.M. Oudenhoven, F. Labohm, M. Mulder, R.A.H. Niessen, F.M. Mulder, P.H.L. Notten, Adv. Mater. 11 (2011) 1–4.
[32] B.J. Neudecker, N.J. Dudney, J.B. Bates, J. Electrochem. Soc. 147 (2000) 517–523.
[33] H. Wang, R.G. Downing, J.A. Dura, D.S. Hussey, in: K. Page, et al. (Eds.), Polymers for Energy Storage and Delivery: Polyelectrolytes for Batteries and Fuel Cells, ACS Symposium Series, American Chemical Society, Washington, DC, 2012, pp. 91–106.

[34] M. Roberts, J.J. Biendicho, S. Hull, P. Beran, G.S. Gustafsson, K.J. Edstrom, J. Power Sources 226 (2013) 249–255.
[35] A. Deb, U. Bergmann, E.J. Cairns, S.P. Cramer, J. Synchrotron Radiat. 11 (2004) 487–504.
[36] A. Deb, U. Bergmann, S.P. Cramer, E.J. Cairns, J. Electrochem. Soc. 154 (2007) A534–A541.
[37] S.C. Chao, Y.C. Yen, Y.F. Song, H.S. Sheu, H.C. Wu, N.L. Wu, J. Electrochem. Soc. 158 (2011) A1335–A1339.
[38] B. Bhushan, Nanotribology and Nanomechanics, third ed., vol. I and II,, Springer, Heidelberg, Germany, 2011.
[39] V. Srinivasan, J. Newman, J. Electrochem. Soc. 151 (2004) A1517–A1529.